

# Physics-informed neural networks viewpoint for solving the Dyson-Schwinger equations of quantum electrodynamics

Rodrigo Carmo Terin<sup>1,\*</sup>

<sup>1</sup>*University of the Basque Country, Department of Computer Science and Artificial Intelligence,  
Intelligent Systems Group, San Sebastian, Spain*

We employ physics-informed neural networks (PINNs) to solve fundamental Dyson-Schwinger integral equations in the theory of quantum electrodynamics (QED) in Euclidean space. Our approach uses neural networks to approximate the fermion wave function renormalization, dynamical mass function, and photon propagator. By integrating the Dyson-Schwinger equations into the loss function, the networks learn and predict solutions over a range of momenta and ultraviolet cutoff values. This method can be extended to other quantum field theories (QFTs), potentially paving the way for forefront applications of machine learning within high-level theoretical physics.

## I. INTRODUCTION AND MOTIVATION

The predictions of the behavior of quantum field theories require an in-depth knowledge of the interactions among fields and particles on different energy scales. One of the theoretical methods to study these interactions is through the famous Dyson-Schwinger Equations (DSEs), which is known for being an infinite set of integral equations fundamental to investigate the infrared region in QFTs, particularly in QED [1, 2]. These integral equations are responsible for describing the dynamics of n-point Green's functions, which have an importance in investigating phenomena like dynamical mass generation, confinement, and the nature of phase transitions in quantum systems [3–6].

In terms of QED, the fermion and photon propagators' DSEs are fundamental in understanding how gauge invariance and chiral symmetry breaking manifest in different energy regimes [7, 8]. It is important to mention that these integral equations form an infinite tower of equations, where each Green function is connected to higher-order ones, and therefore practical applications in general involve truncating the system. The Rainbow-Ladder approximation, for instance, is a commonly used truncation that simplifies the fermion-boson interaction vertex to its lowest-order term [9], a method often employed to study hadronic physics and the high-energy behavior of the quark-gluon

---

\* rodrigo.carmo@ehu.eus

vertex in quantum chromodynamics (QCD)[3].

In recent years, machine learning (ML) algorithms have been recognized as important tools for addressing difficult high-dimensional problems in physics. Among these approaches, the PINNs have emerged as particularly promising. These networks integrate the physical laws governing the system directly into the architecture of the neural network, using loss functions informed by the residuals of the differential equations that must be solved [10–12]. This method has been effectively applied to solve forward and inverse problems involving non-linear partial differential equations (PDEs), enabling high-precision solutions even in the presence of noisy and incomplete data [10, 11].

The wide-range applicability of PINNs covers some physical areas, e.g., the fluid dynamics, where they have been used to reconstruct flow fields from partial observations [13]. In cardiovascular flow modeling, these networks have successfully predicted arterial blood pressure from non-invasive 4D flow Magnetic Resonance Imaging (MRI) data [14], and in plasma physics, they have been used to uncover turbulent transport at the edge of magnetic confinement fusion devices [15]. They have also demonstrated utility in quantum chemistry, where they have been designed to handle high-dimensional quantum many-body problems, such as solving the Schrödinger equation [16].

Moreover, recent advances have expanded the scope of PINNs; for instance, the introduction of Bayesian physics-informed neural networks (B-PINN) has further improved the ability to quantify uncertainty in predictions, making these networks stronger in scenarios where data may be sparse or noisy [17]. In addition, the development of extended PINNs (XPINNs) has enabled more efficient training in parallel architectures [18]. Other extensions of these networks, such as deep operator networks (DeepONets), were responsible for learning mappings between infinite-dimensional function spaces, allowing the solution of operator learning problems [19]. There are more examples like multi-fidelity PINNs that combine data from different sources to increase model accuracy and to reduce computational costs [20]. Furthermore, applications in molecular simulations have led PINNs to accurately predict potential energy surfaces and simulate molecular dynamics [21].

In this work, we extend the use of PINNs to solve the DSEs for the fermion and photon propagators in QED, particularly in Euclidean space. Unlike their conventional applications, which focus on solving PDEs, we employ these networks to tackle the integral equations that govern quantum field theories, such as those represented by DSEs, which are fundamentally more challenging due to their non-local nature and the need to account for all possible interactions in the quantum field [22, 23].

Our adaptation involves incorporating the integral equations of the DSEs directly into the loss

function used during training. By doing so, we preserve the full structure and non-local nature of the DSEs. The neural networks approximate the wave function renormalization, the dynamical mass function, and the photon propagator, and are trained to minimize the discrepancy between their outputs and the solutions to the integral equations. This is achieved by numerically approximating the integrals using deterministic sampling on grids of momentum values and including these computations in the loss function [24–27]. As a consequence, the networks learn solutions that are consistent with both the mathematical form of the DSEs and the underlying physical principles they represent, without modifying the network architecture to include integral operators directly.

This research contributes to a effort to develop physics-informed learning methods capable of solving a wide variety of problems in different scientific domains. By embedding intrinsic physical knowledge within PINNs, this study aims to provide accurate and efficient tools for investigating quantum field dynamics. The results could be a significant step towards new applications of machine learning in physics, from high-energy particle collisions to condensed matter systems.

This manuscript is organized as follows. In Sec. II, we briefly review the background of the DSEs in Euclidean space by presenting the expressions of the fermion and photon propagators. In Sec. III, we introduce the deterministic numerical integration method used to approximate the integral equations and our neural network approach to solve them. We also present the architecture of the neural networks and the training procedure, which includes the selection of hyperparameters and the construction of the loss function. In Sec. IV, we analyze and discuss the results attained from the PINNs for the wave function renormalization, dynamical mass function, and photon propagator on our approach implemented in the previous section. Finally, Sec. V concludes the manuscript, summarizing our findings and suggesting potential directions for future research.

## II. BACKGROUND OF THE DYSON-SCHWINGER EQUATIONS IN EUCLIDEAN SPACE

The Dyson-Schwinger equations provide a non-perturbative approach to determining the Green functions in QFT. In this work, we focus on the DSEs for the renormalized fermion and photon propagators in QED within Euclidean space by following the theoretical formalism developed in our previous work [28]. The transition from Minkowski to Euclidean space is performed via a Wick rotation, which converts the Minkowski time component  $p_0$  into an imaginary component  $p_4 = ip_0$ , simplifying the metric to  $p^2 = p_1^2 + p_2^2 + p_3^2 + p_4^2$ .

In Euclidean space, the inverse fermion propagator  $S_E^{-1}(p)$  can be expressed in terms of the

wave function renormalization  $A(p^2)$  and the mass function  $B(p^2)$ :

$$S_E^{-1}(p) = A(p^2)\not{p} + B(p^2), \quad (1)$$

where  $\not{p} = \gamma_\mu p_\mu$  and  $\gamma_\mu$  are the Euclidean gamma matrices satisfying the anticommutation relation  $\{\gamma_\mu, \gamma_\nu\} = 2\delta_{\mu\nu}$ . Furthermore, to make the DSEs tractable, we employ the Rainbow approximation as our truncation scheme [3, 9]. This simplifies the infinite set of coupled integral equations to a manageable form while retaining essential non-perturbative features of the theory.

The bare fermion-photon vertex is given by:

$$\Gamma^\mu(p, k) = \gamma^\mu, \quad (2)$$

and the dressed photon propagator  $D_{\mu\nu}(k)$  comprises quantum corrections through the photon self-energy.

The functions  $A(p^2)$  and  $B(p^2)$  satisfy the following coupled integral equations derived from the DSEs:

$$B(p^2) = m_{\text{ph}} + g_{\text{ph}}^2 (\Sigma_s(p^2) - \Sigma_s(\mu_F^2)), \quad (3)$$

$$A(p^2) = 1 - g_{\text{ph}}^2 (\Sigma_v(p^2) - \Sigma_v(\mu_F^2)), \quad (4)$$

in which  $\mu_F^2$  is the renormalization scale for the fermion field.

To derive the scalar  $\Sigma_s(p^2)$  and vector  $\Sigma_v(p^2)$  components of the fermion self-energy, we start from the fermion self-energy in Euclidean space:

$$\Sigma(p) = -g_{\text{ph}}^2 \int \frac{d^4 k}{(2\pi)^4} \gamma_\mu S(p-k) \gamma_\nu D_{\mu\nu}(k), \quad (5)$$

where  $S(p-k)$  is the fermion propagator and  $D_{\mu\nu}(k)$  is the photon propagator.

The fermion propagator is expressed in terms of  $A$  and  $B$ :

$$S(p-k) = \frac{-A((p-k)^2)(p \not{+} k) + B((p-k)^2)}{A^2((p-k)^2)(p-k)^2 + B^2((p-k)^2)}. \quad (6)$$

The photon propagator is decomposed into transverse and longitudinal components:

$$D_{\mu\nu}(k) = \left( \delta_{\mu\nu} - \frac{k_\mu k_\nu}{k^2} \right) D(k^2) + \xi \frac{k_\mu k_\nu}{k^4}, \quad (7)$$

where  $D(k^2)$  is the scalar part of the photon propagator, and  $\xi$  is the gauge-fixing parameter.

Substituting  $S(p-k)$  and  $D_{\mu\nu}(k)$  into the expression for  $\Sigma(p)$ , we have:

$$\begin{aligned} \Sigma(p) = & -g_{\text{ph}}^2 \int \frac{d^4 k}{(2\pi)^4} \left[ \gamma_\mu \left( \frac{-A((p-k)^2)(p \not{+} k) + B((p-k)^2)}{A^2((p-k)^2)(p-k)^2 + B^2((p-k)^2)} \right) \gamma_\nu \right] \\ & \times \left[ \left( \delta_{\mu\nu} - \frac{k_\mu k_\nu}{k^2} \right) D(k^2) + \xi \frac{k_\mu k_\nu}{k^4} \right]. \end{aligned} \quad (8)$$

Using the gamma matrix identities:

$$\gamma_\mu \gamma_\nu = \delta_{\mu\nu} + i\sigma_{\mu\nu}, \quad \{\gamma_\mu, \gamma_\nu\} = 2\delta_{\mu\nu}, \quad (9)$$

in which  $\sigma_{\mu\nu} = \frac{i}{2}[\gamma_\mu, \gamma_\nu]$ , and noting that the antisymmetric part ( $\sigma_{\mu\nu}$ ) does not contribute upon integration due to symmetry, we simplify the expression.

We decompose  $\Sigma(p)$  into scalar and vector components:

$$\Sigma(p) = \Sigma_s(p^2)\not{p} + \Sigma_v(p^2). \quad (10)$$

To extract  $\Sigma_s(p^2)$  and  $\Sigma_v(p^2)$ , we perform the gamma matrix algebra and integrate over the loop momentum. The key steps involve collecting terms without gamma matrices after contractions for the Scalar component ( $\Sigma_s(p^2)$ ) and collecting terms proportional to  $\not{p}$  for the vector Component ( $\Sigma_v(p^2)$ ). After performing the contractions and using the symmetry of the integrals, we obtain:

$$\Sigma_s(p^2) = \int \frac{d^4k}{(2\pi)^4} \frac{\left[ 3D(k^2)B((p-k)^2) + \xi \frac{B((p-k)^2)}{k^2} \right]}{A^2((p-k)^2)(p-k)^2 + B^2((p-k)^2)}, \quad (11)$$

$$\Sigma_v(p^2) = \int \frac{d^4k}{(2\pi)^4} \frac{A((p-k)^2)(p-k)^2 \left[ 3D(k^2) + \xi \frac{1}{k^2} \right]}{\left[ A^2((p-k)^2)(p-k)^2 + B^2((p-k)^2) \right] p^2}. \quad (12)$$

It is important to note that the factor of 3 arises from contracting gamma matrices and summing over the four-dimensional Euclidean space indices. Also, the terms involving  $\xi$  stem from the longitudinal part of the photon propagator and explicitly depend on the gauge-fixing parameter. Finally, due to rotational symmetry in Euclidean space, integrals over odd functions of  $k$  vanish, and certain tensor integrals simplify.

The photon propagator satisfies its own Dyson-Schwinger equation:

$$\frac{1}{D(k^2)} = k^2 \left[ 1 - g_{\text{ph}}^2 (\Pi(k^2) - \Pi(\mu_B^2)) \right], \quad (13)$$

where  $\Pi(k^2)$  is the photon self-energy, given by:

$$\Pi(k^2) = \int \frac{d^4p}{(2\pi)^4} F(p^2) F((p-k)^2) \left[ A(p^2)A((p-k)^2)(p^2 - p \cdot k) + 2B(p^2)B((p-k)^2) \right], \quad (14)$$

and

$$F(p^2) = \frac{1}{A^2(p^2)p^2 + B^2(p^2)}. \quad (15)$$

The renormalized mass  $m_{\text{ph}}$  and coupling constant  $g_{\text{ph}}^2$  are related to the bare quantities through:

$$m_{\text{ph}} = m - \frac{g^2 \Sigma_s(\mu_F^2)}{1 - g^2 \Sigma_v(\mu_F^2)}, \quad (16)$$

$$g_{\text{ph}}^2 = \frac{g^2}{1 - g^2 \Sigma_v(\mu_F^2)}. \quad (17)$$

Here,  $g$  and  $m$  are the bare coupling and mass, respectively. Thus, these relations ensure that the physical quantities are finite and properly renormalized on the scale  $\mu_F^2$ .

### III. THE NEURAL NETWORK APPROACH

Our approach focuses on PINNs to approximate the functions  $A(p^2)$ ,  $B(p^2)$ , and  $D(k^2)$ . These are implemented by different networks and trained with loss functions that measure the difference in local discrepancies between sides of DSEs. Namely, we have three distinct neural networks, each one with an input layer, three hidden layers, all using a (tanh) activation function and output nodes. Here are the details for each network:

1. Network for  $A(p^2)$ : Approximates the wave function renormalization of the fermion.
2. Network for  $B(p^2)$ : Approximates the dynamical mass function of the fermion.
3. Network for  $D(k^2)$ : Approximates the photon propagator.

#### A. Numerical Approximation of Integrals

We adopt the Landau gauge, setting the gauge parameter  $\xi = 0$ . This choice simplifies the self-energy expressions by removing terms proportional to  $\xi$ . Consequently, the self-energy components  $\Sigma_s(p^2)$  and  $\Sigma_v(p^2)$  are given by:

$$\Sigma_s(p^2) = \int \frac{d^4 k_E}{(2\pi)^4} \frac{3D(k^2)B((p-k)^2)}{A^2((p-k)^2)(p-k)^2 + B^2((p-k)^2)} R(k^2), \quad (18)$$

$$\Sigma_v(p^2) = \int \frac{d^4 k_E}{(2\pi)^4} \frac{A((p-k)^2)(p-k)^2 \times 3D(k^2)}{A^2((p-k)^2)(p-k)^2 + B^2((p-k)^2)} R(k^2). \quad (19)$$

The integrals appearing in these self-energy calculations involve dependencies on  $p^2$  and  $k^2$ , particularly through expressions such as  $(p-k)^2$ . In our framework, we approximate these integrals

using a deterministic numerical method that involves evaluating the integrand on a grid formed by combinations of sampled momentum values  $p^2$  and  $k^2$  [25, 26].

For each iteration during training, we create grids of sampled values for the momentum variables  $p^2$  and  $k^2$  within a predefined range that reproduces the physical scales of our interest. Specifically, we use uniformly spaced samples within the range  $[0.1, 100.0]$  MeV<sup>2</sup> for both  $p^2$  and  $k^2$ , corresponding to the energy scales of interest:

$$p_i^2 = 0.1 + (i - 1) \Delta_p, \quad i = 1, 2, \dots, N_p, \quad (20)$$

$$k_j^2 = 0.1 + (j - 1) \Delta_k, \quad j = 1, 2, \dots, N_k, \quad (21)$$

where  $\Delta_p = \frac{100.0-0.1}{N_p-1}$  and  $\Delta_k = \frac{100.0-0.1}{N_k-1}$  are the step sizes for  $p^2$  and  $k^2$ , respectively.

The value of  $(p - k)^2$  is computed for each combination of the sampled momenta, forming a two-dimensional grid. The integrands in the self-energy expressions are evaluated at these grid points using the current neural network approximations for  $A(p^2)$ ,  $B(p^2)$ , and  $D(k^2)$ .

The integrals are then approximated by averaging the evaluated integrand values over all sampled points on this grid [25–27]:

$$\Sigma_s(p_i^2) \approx \frac{1}{N_k} \sum_{j=1}^{N_k} \frac{3D(k_j^2)B((p_i - k_j)^2)}{A^2((p_i - k_j)^2)(p_i - k_j)^2 + B^2((p_i - k_j)^2)} R(k_j^2), \quad (22)$$

$$\Sigma_v(p_i^2) \approx \frac{1}{N_k} \sum_{j=1}^{N_k} \frac{A((p_i - k_j)^2)(p_i - k_j)^2 \times 3D(k_j^2)}{A^2((p_i - k_j)^2)(p_i - k_j)^2 + B^2((p_i - k_j)^2)} R(k_j^2). \quad (23)$$

Here,  $N_k$  is the number of sampled momentum points for  $k^2$ , and  $k_j$  represents the  $j$ -th sampled momentum. This numerical approximation replaces the continuous integrals with discrete sums over a deterministic grid, simplifying the computation within our neural network approach.

To approximate these integrals, we use the TensorFlow library [29] for automatic differentiation and parallel computation. The deterministic sampling strategy ensures that our neural networks can learn the behavior of the investigated functions over the entire range of interest. The regulator function  $R(k^2)$  is introduced to handle ultraviolet divergences in the integrals. We choose an exponential regulator of the form:

$$R(k^2) = \exp\left(-\frac{k^2}{\Lambda^2}\right), \quad (24)$$

where  $\Lambda$  is the ultraviolet cutoff scale. This form of  $R(k^2)$  suppresses contributions from large momentum values beyond  $\Lambda$ , ensuring that the integrals remain finite. The choice of  $\Lambda$  balances the

need to include relevant physical contributions while maintaining numerical stability, and therefore, in our simulations, we explore some values of  $\Lambda$  to study its effect on the solutions, choosing  $\Lambda = 0.1, 0.5, 1.0,$  and  $2.0$  GeV.

## B. Training Procedure and Loss Function

Our implementation involves training the neural networks simultaneously using a total loss function that consists of three components, each corresponding to a different Dyson-Schwinger integral equation. The loss function quantifies the difference between the neural network predictions and the expected values given by the DSEs, and it is written as:

$$\begin{aligned} \text{Loss} = & \underbrace{\frac{1}{N_p} \sum_{i=1}^{N_p} \left( B(p_i^2) - [m_{\text{ph}} + g_{\text{ph}}^2 (\Sigma_s(p_i^2) - \Sigma_s(\mu_F^2))] \right)^2}_{\text{Loss}_B} \\ & + \underbrace{\frac{1}{N_p} \sum_{i=1}^{N_p} \left( A(p_i^2) - [1 - g_{\text{ph}}^2 (\Sigma_v(p_i^2) - \Sigma_v(\mu_F^2))] \right)^2}_{\text{Loss}_A} \\ & + \underbrace{\frac{1}{N_k} \sum_{j=1}^{N_k} \left( \frac{1}{D(k_j^2)} - [k_j^2 (1 - g_{\text{ph}}^2 (\Pi(k_j^2) - \Pi(\mu_B^2)))] \right)^2}_{\text{Loss}_D}, \end{aligned} \quad (25)$$

where  $N_p$  and  $N_k$  are the numbers of discretized momentum squared samples used to approximate the continuous integrals and evaluate the neural network predictions against the theoretical values from the DSEs.

The first component,  $\text{Loss}_B$ , is related to  $B(p^2)$ . This term quantifies how closely the network's predictions of  $B(p^2)$  align with the theoretical expression, which depends on the renormalized mass  $m_{\text{ph}}$ , the renormalized coupling constant  $g_{\text{ph}}$ , and the scalar components of the fermion self-energy  $\Sigma_s(p^2)$  and  $\Sigma_s(\mu_F^2)$ . The second term,  $\text{Loss}_A$ , corresponds to  $A(p^2)$ . It evaluates the difference between the predicted and theoretical values of  $A(p^2)$ , which are influenced by the vector components of the self-energy of the fermion,  $\Sigma_v(p^2)$  and  $\Sigma_v(\mu_F^2)$ . Finally, the third component,  $\text{Loss}_D$ , captures the deviation in the photon propagator,  $D(k^2)$ . This loss measures how well the network approximates the inverse of  $D(k^2)$ , as defined by the Dyson-Schwinger integral equation, which incorporates the photon self-energy terms  $\Pi(k^2)$  and  $\Pi(\mu_B^2)$ .

In addition, the physical mass  $m_{\text{ph}}$  and the physical coupling constant  $g_{\text{ph}}$  are computed at a chosen renormalization point for the photon propagator. The expressions (17) account for the renormalization effects due to quantum corrections. Moreover, we employ Adam optimizer [30]



due to its ability to adapt learning rates to individual parameters. Then, the following training parameters are used:

1. **Learning Rate:** The initial learning rate is set to  $\eta = 1 \times 10^{-3}$ .
2. **Number of Epochs:** Training is conducted for a total of 5000 epochs.

During training, we iteratively update the parameters of the neural network and the physical constants  $m_{\text{ph}}$  and  $g_{\text{ph}}$  based on the computed self-energies at each epoch. TensorFlow's automatic differentiation capabilities are used to compute gradients and optimize networks [29].

#### IV. DISCUSSION OF RESULTS

The results attained from the PINNs for  $A(p^2)$ ,  $B(p^2)$ , and  $D(k^2)$  will be presented in this section. Figures 1, 2, and 3 show them for some ultraviolet cutoff values ( $\Lambda = 0.1, 0.5, 1.0$ , and  $2.0$  GeV) over a range of  $p^2$  and  $k^2$ . They enable us to analyze the dependence of these functions on the ultraviolet cutoff  $\Lambda$ .

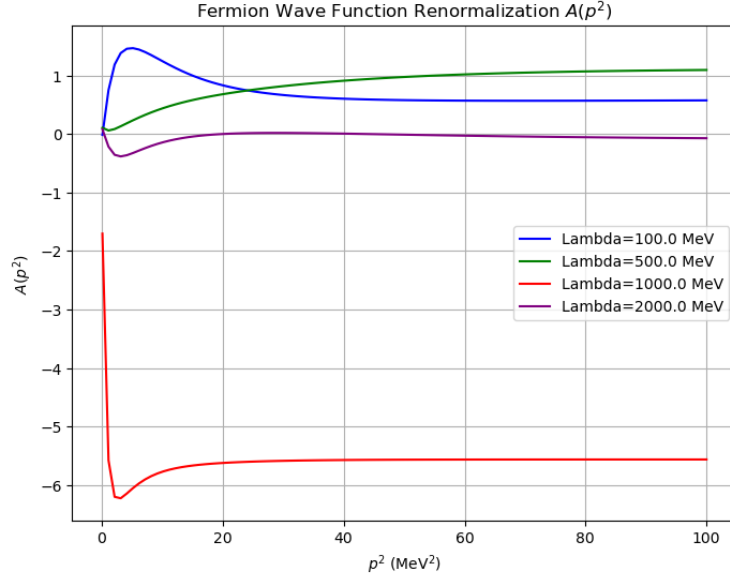


FIG. 1. Results for the fermion wave function renormalization  $A(p^2)$  with different values of  $\Lambda$ .

The parameters  $\Lambda$  used in these simulations correspond to different physical regimes, influencing how quantum fluctuations affect the propagator functions:

1. The renormalization of the fermion wave function  $A(p^2)$  (Fig.1): For low values of  $\Lambda$  (e.g.  $\Lambda = 100$  MeV),  $A(p^2)$  has an evident peak near to the origin, and saturates quickly in the infrared,

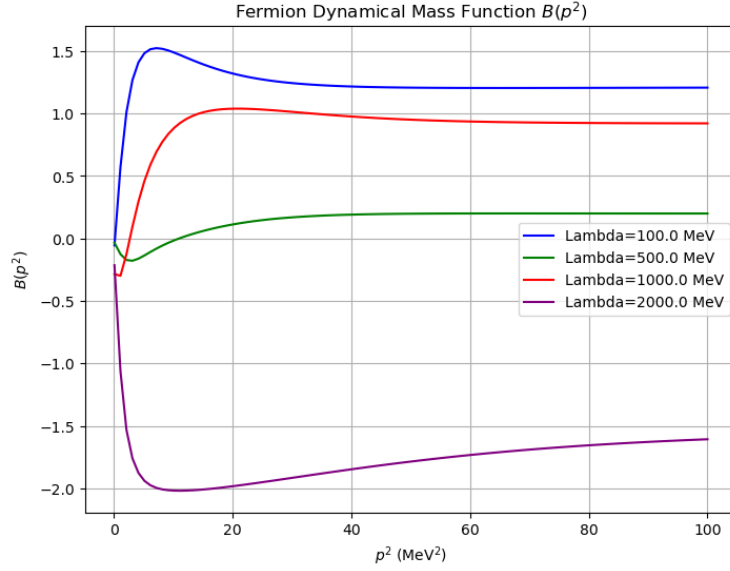


FIG. 2. Results for the fermion dynamical mass function  $B(p^2)$  with different values of  $\Lambda$ .

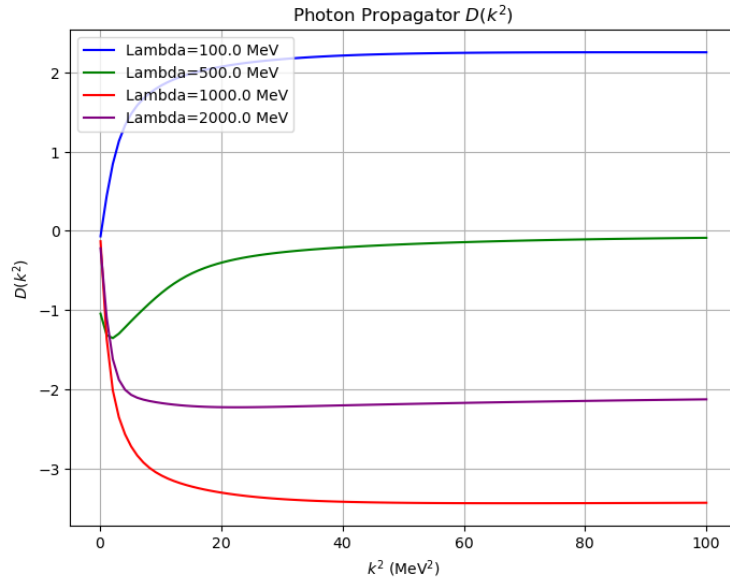


FIG. 3. Results for the photon propagator  $D(k^2)$  with different values of  $\Lambda$ .

making clear the presence of quantum corrections in the infrared momenta. When cutoff is small, this sort of behavior is defined and shows that it is low energy effects which are most dominant. For increasing  $\Lambda$  (e.g.  $\Lambda = 500$  MeV and greater) the  $A(p^2)$  is negative from the start and stays negative for all  $k^2$  indicating positivity violation and confinement like effects. Also, the function becomes increasingly smooth, and the differences decrease. In these cases  $A(p^2)$  converges to a flat profile showing that contributions in the ultraviolet

are dominant, and are thus quenching the dynamical infrared, forcing the behavior towards a more perturbative regime.

2. The fermion dynamical mass function  $B(p^2)$  (Fig.2): At low  $p^2$  (for small cutoffs, e.g.,  $\Lambda = 100$  MeV),  $B(p^2)$  is seen to rise fast, showing that mass generation via non-perturbative effects is large and consistent with dynamical chiral symmetry breaking. This results in the assumption that even the mass term term is not explicit, and then we see the fermion gained heavy mass. This peak in becomes less evident for  $\Lambda = 500$  MeV, where the function approaches saturation at a lower value, however, for higher values of  $\Lambda$  an interesting fact happens since in these values there is the indication of a negative massive behavior of  $B(p^2)$  when  $p^2 \rightarrow 0$ , which confirms that there is the presence of infrared effects in this momentum value.
3. The photon propagator  $D(k^2)$  (Fig.3): In this plot, we can observe the curves of  $D(k^2)$  for different values of the cutoff  $\Lambda$ . Note that for the case  $\Lambda = 0.1$  GeV (blue curve), the propagator is positive from the start and stays positive for all  $k^2$ . This however is not the case for  $\Lambda = 0.5$  GeV where the green curve remains positive only for a certain range and seems to violate positivity at low momenta. In the case of  $\Lambda = 1.0$  GeV red curve and  $\Lambda = 2.0$  GeV purple curve, the positive curves begin with negative values and stay negative, thus violating positivity and suggesting a confinement type effect [31, 32] in all momenta range. These invert below the  $y = 0$  axis hence the conclusion that the propagator takes negative values at certain  $k^2$  regions.

Lastly, the interesting fact from these figures is that almost all curves indicate massive behavior when  $p^2 \rightarrow 0$  and  $k^2 \rightarrow 0$  for  $B(p^2)$  and  $D(p^2)$ , which definitely suggest the presence of dynamical mass generation and confinement effects.

## V. CONCLUSION

In this work, we have used PINNs to tackle the DSEs for QED defined within the bounds of Euclidean space. Our model consisted of three independent neural networks parametrizing the renormalization of the fermion wave function, the dynamical mass function, and the photon propagator. Our neural networks trained to reproduce the solutions of the DSEs as inversions of a variety of ultraviolet cutoffs and momentum. According to the present results we believe that it is possible to reconstruct the DSEs of the model. In particular, it has been observed that by varying

the cutoff values of the ultraviolet parameter, i.e. ( $\Lambda$ ), there is a prominence of the infrared domain that leads to increased changes from the free field behavior in ( $A(p^2)$ ) and the dynamical mass generation rise within ( $B(p^2)$ ). The photon propagator also exhibited behaviors indicative of confinement-like effects.

However, the dependence on  $\Lambda$  raises important reflections on the infrared behavior of the theory. The choice of ultraviolet cutoff influences the extent to which infrared dynamics are manifested in the solutions. Although our method models the impact of  $\Lambda$  within the range studied, it also call attention to the sensitivity of the results to this parameter, especially in the infrared regime. In terms of the computer science perspective, future work could focus on refining our neural network architecture and training procedures or even testing other types of neural networks. Additionally, from a quantum theoretical physics viewpoint, exploring alternative regularization schemes or incorporating known asymptotic behaviors as constraints may capture other nuances of the solutions in the infrared region. Extending this approach to include more sophisticated truncation schemes or applying it to other QFTs, e.g., QCD, could provide other perceptions into non-perturbative phenomena like confinement, dynamical mass generation, and the confinement-deconfinement phase transition.

Finally, our work intends to extend the use of PINNs to solve difficult Dyson-Schwinger integral equations in QFTs. This approach addresses the missing links between machine learning and theoretical physics and offers a new window into the study of quantum field effects and, we hope, also contributes to the larger efforts to develop computational methods in the era of problems relevant to modern physics.

## ACKNOWLEDGMENTS

R. C. Terin acknowledges the Basque Government (projects 214023FMAO, 214021ELCN and IT1504 – 22).

- 
- [1] Freeman J. Dyson. The S matrix in quantum electrodynamics. *Physical Review*, 75:1736–1755, 1949.
  - [2] Julian Schwinger. On the Green’s functions of quantized fields. I. *Proceedings of the National Academy of Sciences*, 37:452–455, 1951.
  - [3] Craig D. Roberts and A. G. Williams. Dyson–Schwinger equations and their application to hadronic physics. *Progress in Particle and Nuclear Physics*, 33:477–575, 1994.

- [4] P. Maris and P. C. Tandy. Bethe-Salpeter study of vector meson masses and decay constants. *Physical Review C*, 60:055214, 1999.
- [5] A. C. Aguilar, A. A. Natale, and P. S. Rodrigues da Silva. Relating a gluon mass scale to an infrared fixed point in pure gauge qcd. *Phys. Rev. Lett.*, 90:152001, Apr 2003.
- [6] O. Oliveira, T. Frederico, and W. de Paula. On the conformal limit of a QED-inspired model. *European Physical Journal C*, 84:851, 2024.
- [7] D.C. Curtis, M.R. Pennington, and D.A. Walsh. On the gauge dependence of dynamical fermion masses. *Physics Letters B*, 249(3):528–530, 1990.
- [8] D. C. Curtis and M. R. Pennington. Nonperturbative truncation of the Schwinger–Dyson equations. *Physical Review D*, 44:536–539, 1991.
- [9] Pieter Maris, Craig D. Roberts, and Peter C. Tandy. Pion mass and decay constant. *Physics Letters B*, 420(3):267–273, 1998.
- [10] P. Perdikaris M. Raissi and G. E. Karniadakis. Physics-informed neural networks: A deep learning framework for solving forward and inverse problems involving nonlinear partial differential equations. *Journal of Computational Physics*, 378:686–707, 2019.
- [11] G. E. Karniadakis et al. Physics-informed machine learning. *Nature Reviews Physics*, 3:422–440, 2021.
- [12] D. I. Fotiadis I. E. Lagaris, A. Likas. Artificial neural networks for solving ordinary and partial differential equations. *IEEE Transactions on Neural Networks*, 9:987–1000, 1998.
- [13] M. Raissi, P. Perdikaris, and G. E. Karniadakis. Hidden fluid mechanics: Learning velocity and pressure fields from flow visualizations. *Science*, 367(6481):1026–1030, 2020.
- [14] G. Kissas et al. Machine learning in cardiovascular flows modeling: Predicting arterial blood pressure from non-invasive 4D flow MRI data using physics-informed neural networks. *Computer Methods in Applied Mechanics and Engineering*, 358:112623, 2020.
- [15] A. Mathews, M. Francisquez, J. W. Hughes, D. R. Hatch, B. Zhu, and B. N. Rogers. Uncovering turbulent plasma dynamics via deep learning from partial observations. *Phys. Rev. E*, 104:025205, Aug 2021.
- [16] David Pfau, James S. Spencer, Alexander G. D. G. Matthews, and W. M. C. Foulkes. Ab initio solution of the many-electron schrödinger equation with deep neural networks. *Phys. Rev. Res.*, 2:033429, Sep 2020.
- [17] Liu Yang, Xuhui Meng, and George Em Karniadakis. B-pinns: Bayesian physics-informed neural networks for forward and inverse pde problems with noisy data. *Journal of Computational Physics*, 425:109913, 2021.
- [18] Ameya D. Jagtap and George Em Karniadakis. Extended physics-informed neural networks (xpinns): A generalized space-time domain decomposition based deep learning framework for nonlinear partial differential equations. *Communications in Computational Physics*, 28(5):2002–2041, 2020.
- [19] Lu Lu, Pengzhan Jin, Guofei Pang, Zhongqiang Zhang, and George Em Karniadakis. Learning nonlinear operators via deepnet based on the universal approximation theorem of operators. *Nature Machine*

- Intelligence*, 3:218–229, 2021.
- [20] X. Meng and G. E. Karniadakis. A composite neural network that learns from multi-fidelity data: Application to function approximation and inverse PDE problems. *Journal of Computational Physics*, 401:109020, 2020.
- [21] Linfeng Zhang, Jiequn Han, Han Wang, Roberto Car, and Weinan E. Deep potential molecular dynamics: A scalable model with the accuracy of quantum mechanics. *Phys. Rev. Lett.*, 120:143001, Apr 2018.
- [22] Reijiro Fukuda and Taichiro Kugo. Schwinger-Dyson Equation for Massless Vector Theory and Absence of Fermion Pole. *Nucl. Phys. B*, 117:250–264, 1976.
- [23] G. V. Efimov. Nonlocal quantum theory of the scalar field. *Communications in Mathematical Physics*, 5:42–56, 1967.
- [24] Paolo Brandimarte. *Numerical Methods in Finance and Economics: A MATLAB-Based Introduction*. John Wiley & Sons, Inc., 2006.
- [25] William H. Press, Saul A. Teukolsky, William T. Vetterling, and Brian P. Flannery. *Numerical Recipes: The Art of Scientific Computing*. Cambridge University Press, 3rd edition, 2007.
- [26] Philip J. Davis and Philip Rabinowitz. *Methods of Numerical Integration*. Academic Press, 2nd edition, May 2014. eBook ISBN: 978-1-4832-6428-8.
- [27] Emanuele Zappala, Antonio Henrique de Oliveira Fonseca, Josue Ortega Caro, Andrew Henry Moberly, Michael James Higley, Jessica Cardin, and David van Dijk. Learning integral operators via neural integral equations. *Nature Machine Intelligence*, 6(9):1046–1062, September 2024.
- [28] Orlando Oliveira, Helena Lessa Macedo, and Rodrigo Carmo Terin. Looking at QED with Dyson–Schwinger Equations: Basic Equations, Ward–Takahashi Identities and the Two-Photon-Two-Fermion Irreducible Vertex. *Few Body Syst.*, 64(3):67, 2023.
- [29] Martín Abadi, Paul Barham, Jianmin Chen, Zhifeng Chen, Andy Davis, Jeffrey Dean, Matthieu Devin, Sanjay Ghemawat, Geoffrey Irving, Michael Isard, et al. Tensorflow: A system for large-scale machine learning. In *12th USENIX Symposium on Operating Systems Design and Implementation (OSDI 16)*, pages 265–283, 2016.
- [30] Diederik P. Kingma and Jimmy Ba. Adam: A method for stochastic optimization. In *Proceedings of the 3rd International Conference on Learning Representations (ICLR)*, 2015.
- [31] Reinhard Alkofer and Lorenz von Smekal. The Infrared behavior of QCD Green’s functions: Confinement dynamical symmetry breaking, and hadrons as relativistic bound states. *Phys. Rept.*, 353:281, 2001.
- [32] Taichiro Kugo and Izumi Ojima. Local Covariant Operator Formalism of Non-Abelian Gauge Theories and Quark Confinement Problem. *Progress of Theoretical Physics Supplement*, 66:1–130, 02 1979.